Fatigue Crack Growth Rate in the Cruciform Specimens under Proportional Tension-Compression

Dariusz Rozumek

Opole University of Technology, Department of Mechanics and Machine Design,
ul. Mikolajczyka 5, 45-271 Opole, Poland

d.rozumek@po.opole.pl

Keywords: mixed mode I + II, stress intensity factor range, biaxial loading, hole, stress ratio.

Abstract. The paper presents the experimental results concerning fatigue life to crack initiation and crack growth in the cruciform plate specimens. The specimens made of 18G2A (S355J0) steel, each with one stress concentrator in form of central hole of 3.0 mm in diameter and without the hole were used. Biaxial fatigue tests were performed under out-of-phase sinusoidal loading with forces control applied to the specimen arms. During the investigations, the number of cycles to initiation was determined and the fatigue crack growth lengths were measured in specimens under different amplitudes of loadings. The tests were performed in the high cycle fatigue regime under tension-compression at Opole University of Technology. The fatigue crack growth was cyclically registered with use of the optical microscope and the digital camera. Depending on the loading level (stress σ_a) and a number of cycles N, in the specimens with hole there were four cracks at the hole edge (in one case, only three cracks occurred), directions of which coincided with mode I. In solid specimens without the hole, initiation and cracks growth to 0.6 mm took place for mixed mode I + II, and next they proceeded to mode I. In solid specimens, there were four cracks, too.

Introduction

Crack growth often takes place in structures subjected to cyclic loadings. This phenomenon can be observed in any devices, such as aeroplanes, vehicles, machines or building structures. Cracks can be caused by various loadings: cyclic or random, uniaxial or multiaxial [1]. The stress, strain and energy criteria are used for calculations of the fatigue life, and the obtained results are compared with the results of experiments. Investigations on initiation and growth of fatigue cracks in cruciform specimens are rarely performed because they require special test stands. The paper [2] presents the tests of plexiglass cruciform specimens with the initiated slots at the angles 45° and 90° to the horizontal axis. The stress intensity factors for modes I and II were calculated with the boundary element method. The authors of [3] tested cruciform specimens and two steels (cyclically hardened and cyclically weakened). The tests included strain control and measurements of the fatigue crack lengths. Initiation and growth of corner fatigue cracks (shapes of ¼ of the circle and ¼ of the ellipse in the specimen section) are described in [4]. The tests were performed at the biaxial fatigue test stand. Plane cruciform specimens were tested under two loading ratios: $P_x : P_y = 1 : 1$ and $1 : 0.5$. Calculations were carried out with the finite element method, too. The paper [5] concerns the fatigue crack growth in cruciform specimens, obtained by welding on the arms to the plane specimens. In [5], initiation and propagation of cracks started in the welded field, and next the crack developed in the native material of the specimen. Crack propagation proceeded perpendicularly to the applied loading (stress) for mode I.

The aim of this paper is to test the fatigue crack growth rate in plane cruciform specimens made of 18G2A steel with central holes, and solid specimens subjected to tension-compression.

Materials and test procedure

Plane cruciform specimens (Fig. 1) were tested. The specimens were made of low-alloy higher-strength steel 18G2A (S355J0) included in the standard PN-EN 10025 of 2002. Steel S355J0 is widely applied for elements of supporting structures, such as bridges, cranes, overhead cranes, high-pressure pipelines of big diameters etc. Its chemical composition and mechanical properties are given in Table 1.

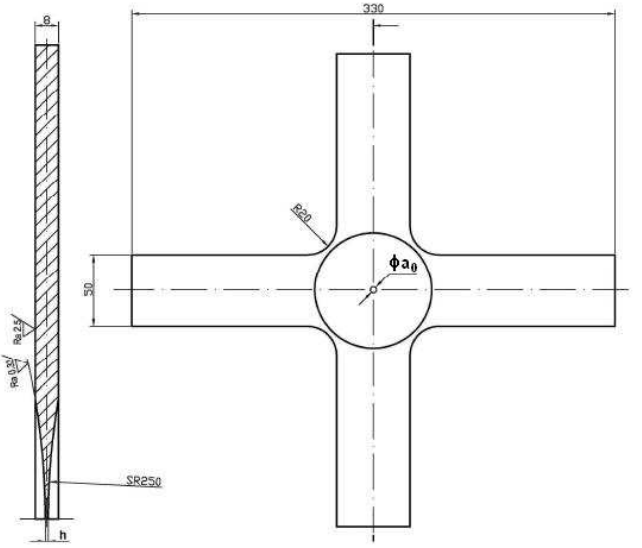

Fig. 1 Specimen for tests of fatigue crack growth, dimensions in mm

Table 1 Chemical composition (in wt %) and monotonic quasi-static properties of the 18G2A steel

Steel	Chemical composition (in wt %)			Mechanical properties
18G2A	0.200C	1.490Mn	0.330Si	σ_y = 357 MPa, σ_u = 535 MPa,
	0.023P	0.024S	0.010Cr	E = 2.10·10^5 MPa, ν = 0.3
	0.010Ni	0.035Cu		

The central part of the specimen, having spherical contour (SR250), was obtained by precise turning. Next, this surface was polished with abrasive paper of decreasing granularity. In the central part of the spherical surface (with the minimum wall thickness h = 1.86 mm) a hole of diameter d = 3.0 mm was made. The theoretical stress concentration factor in the specimen K_t = 2.84, was estimated with use of the model [6]. In the solid specimen (without a hole) the minimum wall thickness was h = 1.25 mm. Coefficients of the cyclic strain curve under tension-compression in the Ramberg-Osgood equation for 18G2A steel are the following [1]: the cyclic strength coefficient K′ = 1323 MPa, the cyclic strain hardening exponent n′ = 0.207. The test results presented in this paper were obtained at Opole University of Technology, in Department of Mechanics and Machine Design [7]. The tests were performed at the fatigue test stand MZPK 100 (Fig. 2) which allowed to realize cyclically and randomly variable histories under static mean value of loading. The control system of the test stand MZPK 100 was elaborated by the research workers from the Department of Mechanics and Machine Design, Opole University of Technology [8]. The tests were performed under loading with the controlled force (P_x, P_y), and constant positions of the intersection points of force directions in axes x, y were kept. Sinusoidal loadings were applied to the specimen arms, they

had the same frequencies f = 13 Hz and similar amplitudes of forces $P_{x,a}$ and $P_{y,a}$ with phase shift by 180^o (coefficient of intercorrelation between force courses P_x (t), P_y (t), shown in Fig. 3 was r = - 1). Loadings of the specimens with holes were: $P_{x,a1\text{-}3}$ = 13.55 kN and $P_{y,a2\text{-}4}$ = 13.30 kN, which corresponded to the nominal amplitude of normal stress $\sigma_{a,1\text{-}3}$ = 105 MPa ($\sigma_{max} = K_t\sigma_a$ = 298 MPa) and $\sigma_{a,2\text{-}4}$ = 103 MPa ($\sigma_{max} = K_t\sigma_a$ = 293 MPa) before the crack initiation. Loadings of the specimens without the holes were: $P_{x,a1\text{-}3}$ = 21.80 kN i $P_{y,a2\text{-}4}$ = 21.50 kN, which corresponded to the nominal amplitude of normal stress $\sigma_{a,1\text{-}3}$ = 209 MPa and $\sigma_{a,2\text{-}4}$ = 206 MPa before the crack initiation. Fatigue tests were performed in the high cycle fatigue regime (HCF) under the stress ratio R = - 1.

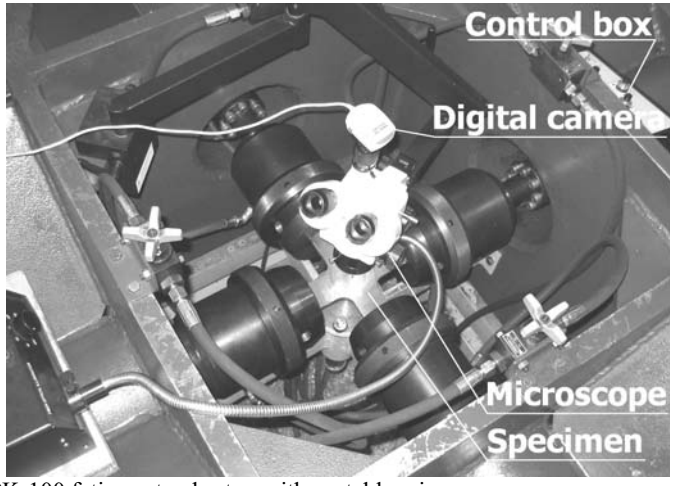

Fig. 2 The MZPK-100 fatigue stand setup with portable microscope

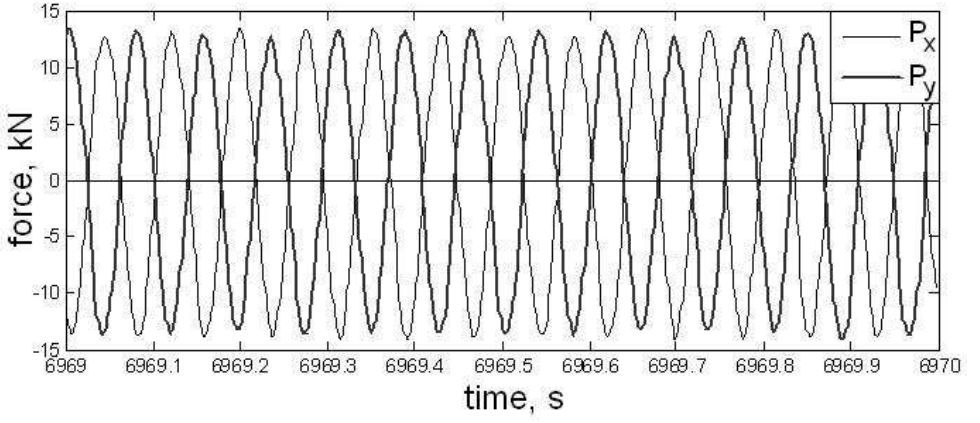

Fig. 3 Fragment of force courses $P_x(t)$, $P_y(t)$ with the intercorrelation coefficient r = - 1

Pictures of one surface of the specimen with fatigue cracks were cyclically registered with the optical microscope (magnification 7x) and the digital camera (0.0085 mm/pixel). The pictures were used for measurements of the fatigue crack lengths a. While tests, also the number of loading cycles N was registered. Strains were measured with rosettes of the measuring base 1 mm.

Experimental results and discussion

The tests were performed under controlled loading. The number of cycles to the crack initiation N_i, i.e. to occurrence of an apparent crack of length $a_i = 0.07 \div 0.20$ mm, was determined and the fatigue crack lengths were measured. In the specimens with holes and the solid specimens usually four cracks for mode I could be seen (see Fig. 4). In one case, three cracks were in the specimen with the central hole. The cracks shown were loaded by similar force amplitudes, but the maximum stresses for the cracks a_1 and a_3 were shift in phase by 180^o related to the stresses for a_2 and a_4. In the specimen with a hole shown in Fig. 4a the cracks developed for mode I. In the solid specimen shown in Fig. 4b the cracks developed for mixed mode I + II (for short cracks of lengths to a = 0.56 mm at the angle about 31° to the y axis). Then, the cracks developed for mode I. In the same specimen and under the same loading, particular cracks initiated under different numbers of cycles N_i (Fig. 5). A characteristic feature of the observed cracks, independent of loading level, was stabilization of the crack growth rate for specimens with holes at the length $a \geq 1$ mm (Fig. 5a), and for solid specimens – at the length $a \geq 3$ mm (Fig. 5b). Comparing the test results shown in Fig. 5 (symbols are used, ◇ - a_1, Δ - a_2, □ - a_3, ∇- a_4) for the curves a = f (N), we can notice different shapes of the curves at the initial stage of crack growth. In the case of the specimens with holes, the shape of the curve is similar to logarithmic curves, and for the solid specimens (without a hole) the test results form a shape of exponential curves.

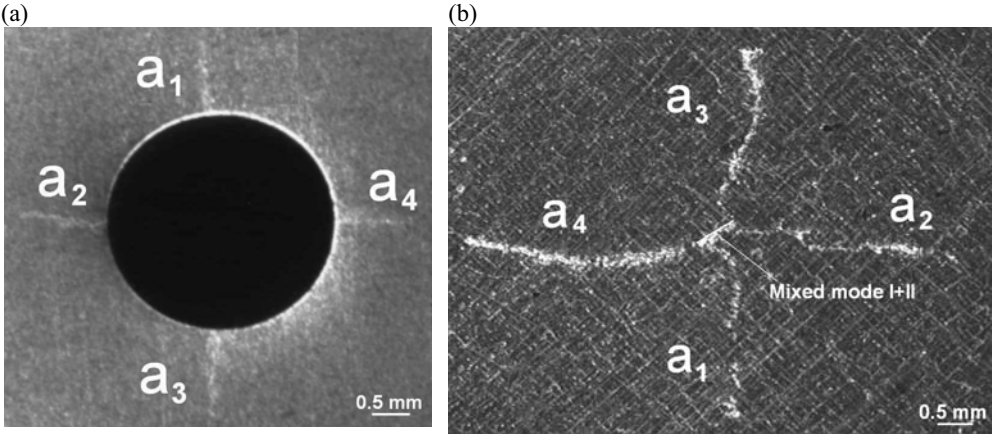

Fig. 4 Crack growth in specimens (a) with hole, (b) without hole

Fig. 5 contains values of the fatigue crack growth rate determined with the use of linear regression with the least square method for crack lengths greater than 1 mm (specimen with the hole) and greater than 3 mm (solid specimen). In all the cases, the coefficients of correlation are $r = 0.995 \div 0.999$, and the cracking rates have similar values for the considered specimen (see Fig. 5).

(a)

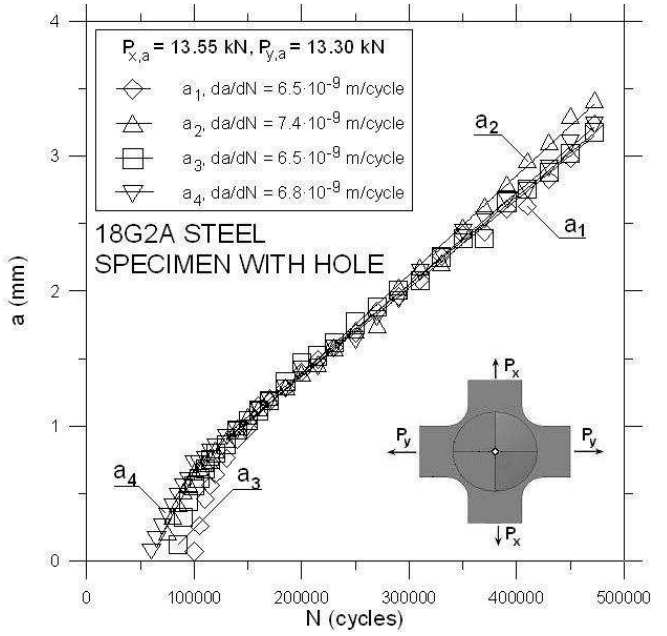

(b)

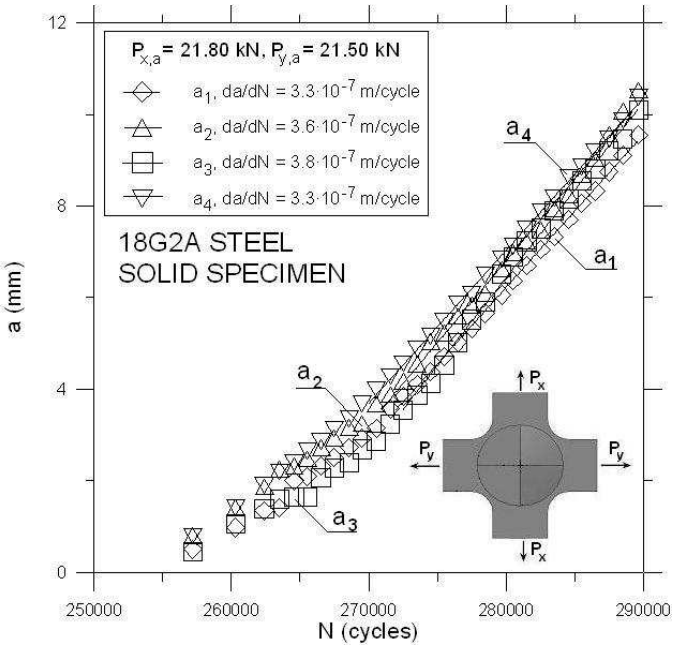

Fig. 5 Dependencies of fatigue crack length a versus number of cycles N for specimens: (a) with hole, (b) without hole

Characteristics of the fatigue cracking growth rates da/dN versus the range of stress intensity factor ΔK for loadings along axes x and y respectively are presented in Fig. 6. The analytic approximate method was applied for description of fatigue crack growth rate because of a complicated shape of the specimen. In calculations, the cruciform specimen (biaxially loaded) was replaced by two plane specimens uniaxially loaded along x and y axes. During tests, when the x axis was subjected to tension, the y axis was subjected to compression and inversely (Fig. 3). Moreover, preliminary calculations of stresses were performed according to the finite element method to the moment of the crack initiation and with the FRANC3D software. The calculation results obtained with the analytic and numerical methods were similar (the relative error did not exceed 15%). In Fig. 6a we can see increase of cracking growth rate from da/dN = $4.0 \cdot 10^{-8}$ m/cycle to da/dN = $5.8 \cdot 10^{-8}$ m/cycle, which corresponds to the initial constant thickness of the specimen h = 1.86 mm. Next, we observe decrease of the cracking growth rate to about da/dN = $1.8 \cdot 10^{-8}$ m/cycle and its stabilization within da/dN = $1.8 \cdot 10^{-8} \div 1.0 \cdot 10^{-8}$ m/cycle. Such behaviour of cracks can be explained by decrease of stresses caused by the increase of the specimen thickness, which stabilizes an increase of the fatigue cracking growth rate. Similar behaviour could be observed in the case of all tested specimens with holes.

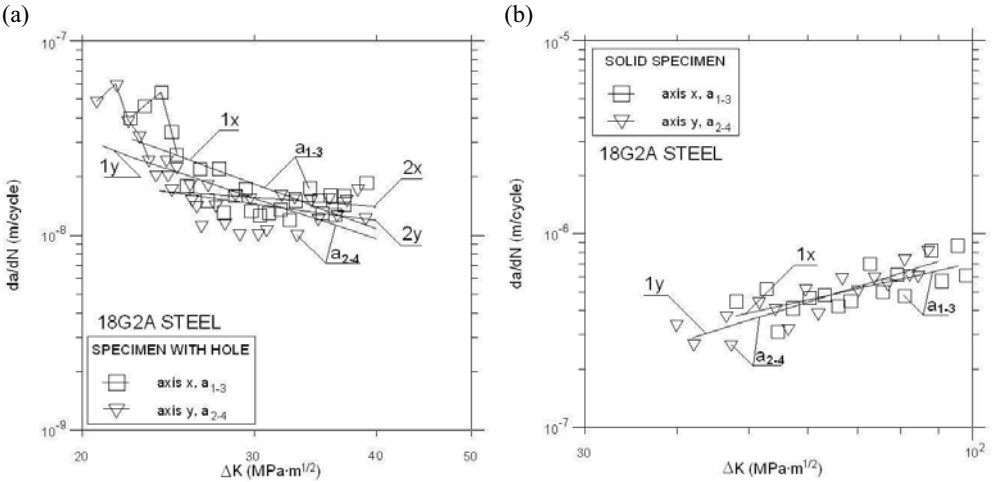

Fig. 6 Comparison of the experimental results with calculated ones according to Eq. (1) for specimens: (a) with hole, (b) without hole

In the solid specimen (Fig. 6b), typical behaviour of cracks (progressive increase of cracking) was observed in both x and y axes. The experimental results shown in Fig. 6 of crack growth rate as a function of the stress intensity factor range were described with the Paris equation [9]

$$\frac{da}{dN} = C(\Delta K)^m, \tag{1}$$

where $\Delta K = K_{max} - K_{min}$.

For the specimens with the holes the range of the stress intensity factor for mode I is calculated from

$$\Delta K = Y_1 \Delta\sigma_{nom} \sqrt{\pi(a + a_0)}, \tag{2}$$

and for the solid specimens we use the following equation

$$\Delta K = Y_2 \Delta\sigma_{nom} \sqrt{\pi a}\ , \tag{3}$$

where $\Delta\sigma_{nom}$ is the stress range under tension and compression ($\Delta\sigma_{nom} = 2\sigma_a$, $\sigma_a = P_a/S$, rectangular cross-section S = wh, w = 50 mm – specimen width), a_0 - slot length, a - crack length. Correction factors [10] for the specimen with hole $Y_1 = 1 - 0.1\left(\frac{2(a_0 + a)}{w}\right) + \left(\frac{2(a_0 + a)}{w}\right)^2$ and for the specimen without hole $Y_2 = 1 + 0.128\left(\frac{2a}{w}\right) - 0.288\left(\frac{2a}{w}\right)^2 + 1.525\left(\frac{2a}{w}\right)^3$.

The range of short fatigue cracks (about 50 ÷ 600 μm in length) is characterized by Eq. (3) [11]. The cracks developed for the mixed mode I + II (Fig. 4b). Crack growth for the solid specimen and loading along the axis y is the sum of the crack lengths for mixed mode I + II multiplied by cosinus of the angle plus lengths of increment of particular cracks for mode I. The crack lengths for loading in the axis x and mixed mode I + II should be multiplied by sinus of the angle plus lengths increment of particular cracks in this axis. Comparing cracking growth rates for the specimens with holes and without holes, we can notice that cracking growth rates for the solid specimens are higher. The experimental coefficients C and m from Eq. (1) were calculated with the least square method and shown in Table 2. In the case of the specimen with the hole, the coefficients C and m were calculated for all the points of cracking growth rates shown in Fig. 6 (curves 1x and 1y) and for the cracking growth rates not including the five initial points of increase and decrease of cracking growth rates (curves 2x and 2y). From Table 2 it appears that the coefficients C and m for curves 1x, 1y, and 2x, 2y are different. Moreover, we can see that the coefficient of inclination of the straight line m for the specimen with the hole takes negative values, and for the solid specimen it is positive. The test results for cyclic tension-compression include a relative error not exceeding 20% (specimens with the hole not including the first five measuring points) at the 5% significance level for the correlation coefficients r given in Table 2. The coefficients of correlation in all the cases are high, so there is a significant correlation between the experimental results with the assumed model represented by Eq. (1).

Table 1 Coefficients C, m of Eq. (1) and correlation coefficients r for the curves shown in Fig. 6

Figure	C m(MPa·m$^{1/2}$)$^{-m}$/cycle	m	r
Fig. 6a, curve 1x	$1.005 \cdot 10^{-5}$	-1.854	-0.814
Fig. 6a, curve 2x	$5.483 \cdot 10^{-8}$	-0.369	
Fig. 6a, curve 1y	$4.688 \cdot 10^{-6}$	-1.679	-0.788
Fig. 6a, curve 2y	$1.503 \cdot 10^{-7}$	-0.687	
Fig. 6b, curve 1x	$1.371 \cdot 10^{-8}$	0.856	0.815
Fig. 6b, curve 1y	$3.443 \cdot 10^{-9}$	1.187	0.893

While tests, strains were measured with rosettes in order to check a degree of bending of the specimen in the points of the fatigue crack growth. From the obtained results it appears that the strain amplitude coming from bending is very low (2.6 % of the total strain) and can be disregarded.

Conclusions

The presented results of the fatigue crack growth in the cruciform plate specimens subjected to tension-compression loading allow to formulate the following conclusions:

1. Initiation and growth of fatigue cracks in the specimens with the holes occurred at the hole edge under different number of cycles for mode I.
2. In the solid specimens, initiation and growth of the cracks occured first (to crack length about 0.6 mm) for the mixed mode I + II, next the cracks developed for mode I.
3. In the tested specimens behaviour of the fatigue crack growth rate varied. It was caused by occurrence of the stress concentration in the specimens with holes.

References

[1] D. Rozumek and E. Macha: Opole University of Technology, (2006), p. 196 (in Polish)

[2] K. Molski and W. Będkowski: 5th Int. Conference on Biaxial/Multiaxial Fatigue and Fracture, edited by Macha E. and Mróz. Z., Technical University of Opole, (1997)

[3] M. Sakane and M. Ohnami: Third Int. Conference on Biaxial/Multiaxial Fatigue, MPA Universitat Stuttgart (1989)

[4] S.M. Shen & Z.L. Feng: Int. J. Pres. Ves. & Piping, Vol. 68 (1996), pp. 319-324.

[5] I.T. Kim and S. Kainuma: Int. J. Pres. Ves. & Piping, Vol. 82 (2005), pp. 807-813.

[6] A. Thum, C. Petersen, O. Swenson: Verformung, Spannung und Kerbwirkung. VDI, (1960)

[7] A. Karolczuk, D. Rozumek, C.T. Lachowicz, J. Słowik: Przegląd Mechaniczny, Vol. 83 (2007), pp. 69-76 (in Polish)

[8] L. Kasprzyczak, J. Słowik, E. Macha: Scientific Papers of the Opole University of Technology, Vol. 83 (2005), pp. 69-76 (in Polish)

[9] P.C. Paris and F. Erdogan: J. of Basic Eng., Trans. ASME, Vol. 85 (1960), pp. 528-534.

[10] S. Kocańda and J. Szala: PWN, Warsaw, 1997 (in Polish)

[11] D. Kocańda, S. Kocańda, E. Łunarska, J. Mierzyński: Materials Science, Vol. 41 (2005), pp. 304-308.